



Petrogenesis of the Yangzhuang Nb- and Ta-rich A-type granite porphyry in West Junggar, Xinjiang, China



Wei Mao ^{a,b}, Xiaofeng Li ^{a,*}, Guo Wang ^c, Rong Xiao ^d, Mou Wang ^c, Yanlong Li ^c, Manchuan Ren ^c, Yanping Bai ^e, Feng Yang ^e

^a State Key Laboratory of Ore Deposit Geochemistry, Institute of Geochemistry, Chinese Academy of Sciences, Guiyang, Guizhou 550002, China

^b University of Chinese Academy of Sciences, Beijing 100049, China

^c 216 Team, China National Nuclear Corporation, Urumqi 830011, China

^d Hunan Institute of Geological Survey, Changsha 410116, China

^e College of Earth Sciences, Guilin University of Technology, Guilin 541004, China

ARTICLE INFO

Article history:

Received 1 January 2014

Accepted 31 March 2014

Available online 12 April 2014

Keywords:

Yangzhuang granite porphyry

A-type granite

Nb

Ta

Ridge subduction

West Junggar

ABSTRACT

West Junggar is featured with a wide spread of Late Carboniferous–Early Permian A-type granites. Systematic comparison of the Yangzhuang granite porphyry and the regional coeval A-type granites (RCAG) shows that: (1) all the Late Carboniferous–Early Permian A-type granites are of the A₂ group except the Yangzhuang granite porphyry; (2) the Nb and Ta contents of the Yangzhuang granite porphyry are nearly 10 times that of the RCAG while Ti content is more depleted; (3) εNd (*t*) of the Yangzhuang granite porphyry is slightly lower and the Sr isotope has a wider range relative to the RCAG. Previous research revealed that highly incompatible elements including Nb and Ta can be transferred into the mantle wedge by precipitation of amphibole from the ascending fluids generated by dehydration of subducted slab. It is inferred that enhanced heat flux brought by the Late Carboniferous ridge subduction decomposed amphibole in the mantle wedge to generate Nb and Ta-rich melt and finally produced the Yangzhuang granite porphyry.

© 2014 Elsevier B.V. All rights reserved.

1. Introduction

A-type granites, originally defined as alkaline, anhydrous and anorogenic granites by Loiselle and Wones (1979), have been extensively studied due to their distinctive compositions, origins and tectonic settings (Bonin, 2007; Clemens et al., 1986; Collins et al., 1982; Eby, 1990, 1992; Han et al., 1997; King et al., 1997; Loiselle and Wones, 1979; Whalen et al., 1987). Eby (1992) subdivided A-type granites into two chemical groups by elemental ratios. The A₁ group represents mantle derived magma differentiates with the same origins that produce oceanic-island, intraplate, and rift-zone magmas, while magmas of the A₂ group are partially melted lithosphere by continental margin or island-arc magmatism (Eby, 1992). Although major progress has been made during the past few decades, the concept has proven controversial and “A-” remains ambiguous because these magmas can be generated in various tectonic settings (Bonin, 2007; Whalen, 2005). Origins of A-type granite magmas proposed by different petrogenetic schemes vary from highly fractionated products of direct mantle source with or

without continental contamination (Han et al., 1997; Jung et al., 1998; Litvinovsky et al., 2002; Mushkin et al., 2003; Turner et al., 1992; Volkert et al., 2000) to hybridization of mantle-derived magmas with crustal melts (Bédard, 1990; Mingram et al., 2000; Wickham et al., 1996; Yang et al., 2006) to partial melting of the lower crust (Clemens et al., 1986; Collins et al., 1982; King et al., 1997; Whalen et al., 1987).

The Central Asian Orogenic Belt (CAOB), formed by successive accretion of arc complexes in the Phanerozoic (Sengör et al., 1993), is bordered by the North China–Tarim craton on the south. The West Junggar region located in the southern part of the CAOB is characterized by the wide spread of Late Paleozoic A- and I-type granites with highly depleted isotopic signatures (Chen and Arakawa, 2005; Han et al., 1997, 2006; Shen et al., 2011; Tang et al., 2010a).

Most of the reported Late Carboniferous–Early Permian A-type granites in the West Junggar region are geochemically similar to the A₂ group (Shen et al., 2011) except the Yangzhuang granite porphyry. Zhang and Zhang (2014) reported the zircon U–Pb dates, Sr–Nd–Hf isotopic compositions, and major element and trace element geochemistry studies of the Yangzhuang granite porphyry. They concluded that the Yangzhuang granite porphyry was derived from an oceanic island basalt-like mantle source during the southward subduction of the Irtysh–Zaysan oceanic lithosphere beneath the Zharma–Saur arc. However, a systematic comparison of the Yangzhuang granite porphyry and the regional coeval A-type granites (RCAG) reveals that the Yangzhuang

* Corresponding author at: Institute of Geochemistry, Chinese Academy of Sciences, 46 Guanshui Road, Guiyang, Guizhou 550002, China. Tel.: +86 18811080229.

E-mail addresses: dzmaowei@163.com (W. Mao), x-f-li@hotmail.com (X. Li).

granite porphyry is featured with strong enrichment of Nb and Ta and depletion of Ti. Combined with the Sr–Nd–Pb isotope signature, the northwestward ridge subduction model is preferred to interpret the formation of A-type granites in West Junggar in the Late Carboniferous to Early Permian. The enrichment of Nb and Ta in the Yangzhuang granite porphyry is attributed to three stages of metasomatism in the mantle wedge and the following ridge subduction.

2. Geological setting

2.1. Geology of West Junggar

The West Junggar region located on the southern part of the Altai Orogen can be divided into two parts (Yang et al., 2012) (Fig. 1). The northern Junggar mainly consists of two parallel E–W trending volcanic belts separated by the E–W trending Hongguleleng–Hebukesaier–Kujibai ophiolite belt (Chen et al., 2010; Shen et al., 2012). The Xuemisitan (or Xiemisitai) volcanic belt on the south is the eastern part of the Boshchekul–Chingiz volcanic arc formed in southward subduction of Junggar oceanic crust in the Silurian–Early Devonian (Shen et al., 2012; Zhao and He, 2013). The closure of the oceanic basin between the Xuemisitan and Zharma–Saur volcanic arcs took place before the Late Devonian (~380 Ma, Filippova et al., 2001). The Zharma–Saur volcanic arc on the north, mainly composed of calc-alkaline basalts and basaltic andesites, is the product of southward subduction of the Irtysh–Zaysan oceanic lithosphere during the Devonian–Early Carboniferous (Didenko and Morozov, 1999; Vladimirov et al., 2008). Ages of stitching plutons indicate that the Irtysh–Zaysan oceanic basin closed in the Late Carboniferous (Chen et al., 2010; Han et al., 2010; Kuibida et al., 2009).

The southern Junggar consists mainly of the Devonian to Carboniferous sandstone and volcanic rocks, including basalt, andesitic basalt, andesite, and minor felsic tuff (Yang et al., 2012). They are intruded by dioritic stocks at ~315 Ma (Tang et al., 2009) and alkali-feldspar granite batholiths at ~300 Ma (Table 1) (Chen and Jahn, 2004; Chen et al., 2010; Geng et al., 2009; Han et al., 2006; Su et al., 2006). The NE-trending Dalabute fault is a suture zone formed by the collision of Kulumudi terrane and Karamay terrane (Yang et al., 2012; Zhang et al., 2011a, 2011b). Ages of the granite batholiths including Hongshan (301 Ma), Karamay (295 Ma), Tiechanggou (308 Ma), Hatu (302 Ma), Akbastao (303 Ma), Miaoergou (308 Ma), Kulumusu (302 Ma), and Sailike (304 Ma) combined with coeval mafic intrusions indicate that tremendous magmatism took place in the Late Carboniferous to Early Permian (Geng et al., 2009).

A post collisional model was first proposed to interpret the formation of the granitic batholiths in West Junggar (Chen and Arakawa, 2005; Han et al., 1997, 1999), but now it is highly challenged by the lithofacies paleogeographical studies and the paleomagnetic research which revealed that a remnant oceanic basin still existed in the West Junggar region until 300 Ma ago (Choulet et al., 2011; Wang, 2006; Wang et al., 2007a). An ocean ridge subduction model proposed by Geng et al. (2009) has been gradually accepted to interpret the extensive Late Carboniferous magmatism in West Junggar (Geng et al., 2011; Tang et al., 2009, 2010a, 2010b; Yang et al., 2012; Yin et al., 2010, 2011).

2.2. Geology of the Baiyanghe Be–U deposit

The Yangzhuang granite porphyry is located on the southern border of the middle part of the Xuemisitan volcanic belt (Fig. 1). Stratigraphic

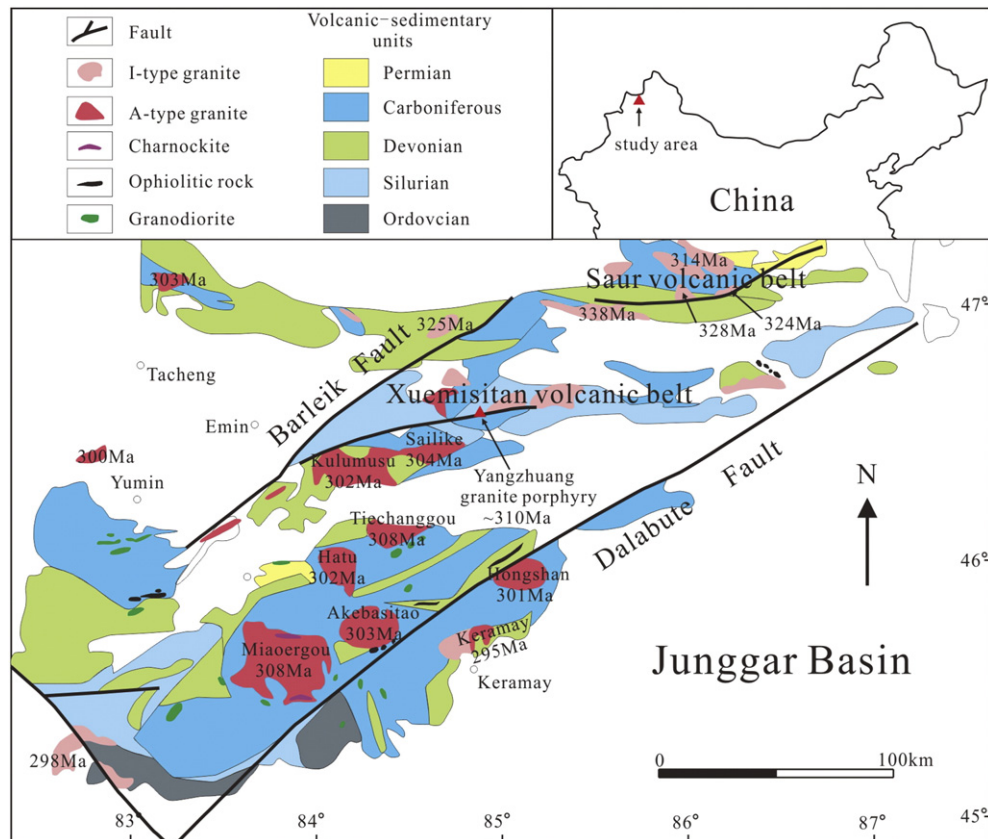


Fig. 1. Geological map of West Junggar, Xinjiang, Northwest China. Modified after Chen et al. (2010). Age data from Chen et al. (2010), Geng et al. (2011), Shen et al. (2012), and Zhang and Zhang (2014).

Table 1

Ages of the Yangzhuang granite porphyry and the RCAG.

Samples	Rock type	Analytical methods	Ages (Ma)	References
Miaogou	Alkali-feldspar granite	SHRIMP Zircon U-Pb	308 ± 6	Geng et al. (2009)
Miaogou	Alkali-feldspar granite	LA-ICP-MS Zircon U-Pb	305 ± 2	Su et al. (2006)
Miaogou	Alkali-feldspar granite	LA-ICP-MS Zircon U-Pb	306.4 ± 8.8	Gao et al. (2006)
Miaogou	Alkali-feldspar granite	SHRIMP Zircon U-Pb	327 ± 7	Han et al. (2006)
Karamay	Alkali-feldspar granite	LA-ICP-MS Zircon U-Pb	296 ± 4	Su et al. (2006)
Karamay	Alkali-feldspar granite	SHRIMP Zircon U-Pb	295 ± 4.6	Han et al. (2006)
Akbastao	Alkali-feldspar granite	SHRIMP Zircon U-Pb	290 ± 8	Han et al. (2006)
Akbastao	Alkali-feldspar granite	Rb-Sr isochron	302 ± 8	Li et al. (2000)
Akbastao	Alkali-feldspar granite	LA-ICP-MS Zircon U-Pb	303 ± 3	Su et al. (2006)
Akbastao	Alkali-feldspar granite	LA-ICP-MS Zircon U-Pb	305 ± 4	Geng et al. (2009)
Akbastao	Alkali-feldspar granite	LA-ICP-MS Zircon U-Pb	318 ± 2.9	Gao et al. (2006)
Hongshan	Alkali-feldspar granite	LA-ICP-MS Zircon U-Pb	301 ± 4	Su et al. (2006)
Tiechanggou	Alkali-feldspar granite	SHRIMP Zircon U-Pb	308.4 ± 4	Han et al. (2006)
Hatu	Alkali-feldspar granite	Rb-Sr isochron	287 ± 29	Li et al. (2000)
Hatu	Alkali-feldspar granite	SHRIMP Zircon U-Pb	302.4 ± 4	Han et al. (2006)
Kulumusu	Alkali-feldspar granite	LA-ICP-MS Zircon U-Pb	302 ± 2	Chen et al. (2010)
Sailike	Alkali-feldspar granite	LA-ICP-MS Zircon U-Pb	304 ± 2	Chen et al. (2010)
Jiangbule	Alkali-feldspar granite	LA-ICP-MS Zircon U-Pb	309 ± 2	Xu et al. (2012)
Taergen	Alkali-feldspar granite	LA-ICP-MS Zircon U-Pb	309 ± 4	Xu et al. (2012)
Taergen	Alkali-feldspar granite	SHRIMP Zircon U-Pb	296 ± 3	Song et al. (2011)
Yangzhuang	Granite porphyry	SHRIMP Zircon U-Pb	309.3	Ma et al. (2010)
Yangzhuang	Granite porphyry	LA-ICP-MS Zircon U-Pb	313 ± 2.3	Zhang and Zhang (2014)

sequences in the Baiyanghe area include intermediate-acidic volcanic and pyroclastic rocks with minor basic tuff of the Late Devonian Tarbagatay Group; shale, limestone, siliceous shale, sandstone and conglomerate of the Early Carboniferous Hebukehe Group; sandstone, basic-intermediate volcanic and pyroclastic rocks of the Early Carboniferous Heishantou Group (Mao et al., 2013; Wang et al., 2012; Zhang and Zhang, 2014). NW-SE trending diabase and diorite dikes crosscutting the Yangzhuang granite porphyry are widely developed (Fig. 2).

The Yangzhuang granite porphyry exhibits porphyritic structure with about 3–8% quartz and K-feldspar phenocrysts (Fig. 3). Anhedral quartz and slightly altered euhedral feldspar phenocrysts are identified under a microscope (Fig. 3b, c). The matrix is composed of microcrystalline quartz, K-feldspar, plagioclase and minor amounts of biotite. The accessory minerals were mostly magnetite with hematitization. Zircon U-Pb dating of the Yangzhuang granite porphyry yielded the intrusion age of ~310 Ma (Ma et al., 2010; Zhang and Zhang, 2014).

The Baiyanghe Beryllium-Uranium deposit is mainly situated in the contact zone of the Yangzhuang granite porphyry and the Late Devonian Tarbagatay Group on the north (Fig. 2), and it is reported to be one of the largest Be-U deposits in Asia (Wang et al., 2012;

Zhang and Zhang, 2014). The age of the Be-U mineralization is 303 Ma according to the muscovite ^{40}Ar - ^{39}Ar dating (Li et al., 2013). The beryllium occurs as bertrandite and the majority of the original uranium minerals (pitchblende) were altered to uranophane (Wang et al., 2012). The Yangzhuang granite porphyry was inferred to be the source of Be and U because its average contents of Be and U reached 13 ppm and 17 ppm, respectively (Mao et al., 2013; Wang et al., 2012). The Be-U deposit was formed in a hydrothermal system heated by the intermediate-basic dikes intruded in the Yangzhuang granite porphyry (Mao et al., 2013).

3. Sample collection and analytical methods

3.1. Sample collection

The alteration zone of the Baiyanghe Be-U deposit is constrained in the contact zone between the Yangzhuang granite porphyry and the Tarbagatay Group on the north. Fresh samples from outcrops and drillholes far from the alteration zone are collected to minimize the influence of alteration (Fig. 2). These samples include outcrop samples

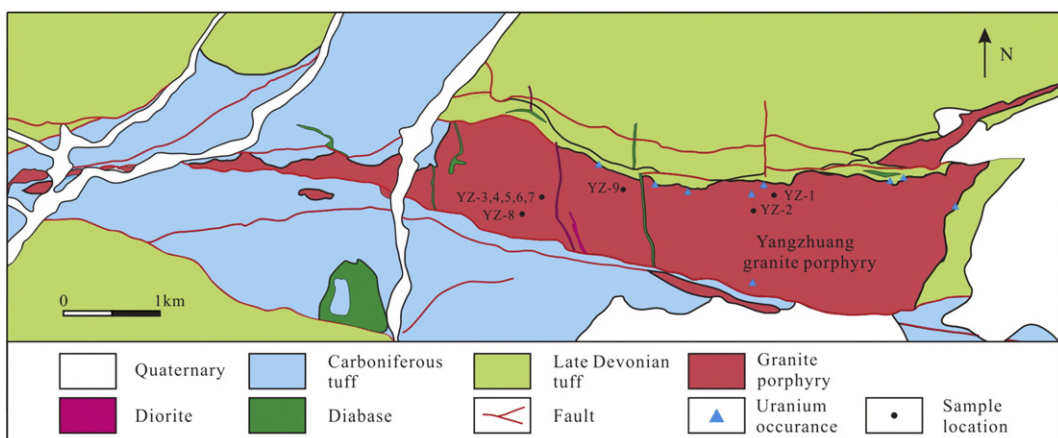


Fig. 2. Geological map of the Baiyanghe Be-U deposit, Xinjiang, Northwest China. Modified after Wang et al. (2012).

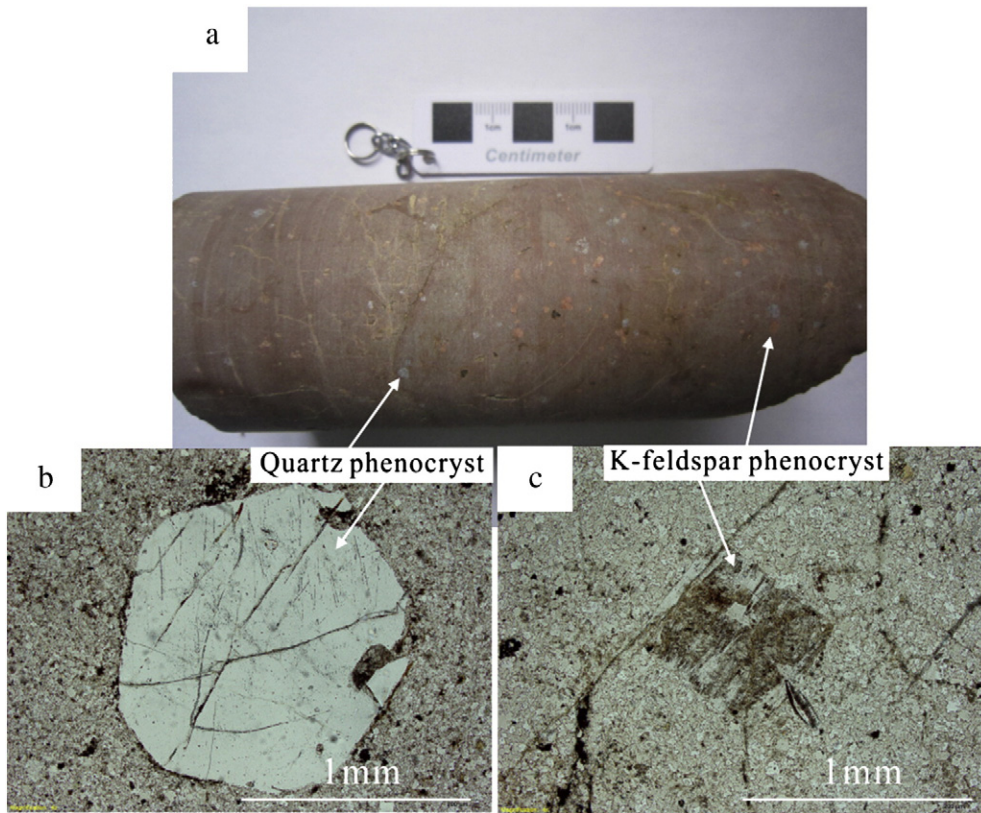


Fig. 3. Microscopic photos of the Yangzhuang granite porphyry. (a) Hand specimen; (b) Quartz phenocryst; (c) Slightly altered K-feldspar phenocryst.

YZ-1, YZ-2, YZ-8, and YZ-9 and samples YZ-3, YZ-4, YZ-5, YZ-6, and YZ-7 collected from drillhole ZK7702 at depths of 37.0 m, 54.9 m, 99.0 m, 132.9 m, and 183.1 m, respectively.

3.2. Analytical methods

The major element compositions were carried out by a Philips PW2404 wavelength dispersive X-ray fluorescence spectrometry (XRF) on fused glass disk at the Beijing Research Institute of Uranium Geology (BRIUG). The analytical precision for major element determination was better than 1%. Sample powders for trace element analyses were digested with mixed $\text{HNO}_3 + \text{HF}$ acid in steel-bomb coated Teflon beakers to assure the complete dissolution of refractory minerals. Trace elements are determined by a Finnigan Element II ICP-MS at the BRIUG following the procedures described by Li (1997). The analytical precision for trace elements was between 5% and 10% for trace elements, depending on the concentration level of a specific element.

Sr–Nd–Pb isotopes were determined by an Isoprobe-T thermal ionization mass spectrometry at the BRIUG following the procedures of GB/T17672-1999. The $^{143}\text{Nd}/^{144}\text{Nd}$ ratios were normalized to $^{146}\text{Nd}/^{144}\text{Nd}_{\text{standard}} = 0.7219$ while the $^{87}\text{Sr}/^{86}\text{Sr}$ ratios were normalized with $^{88}\text{Sr}/^{86}\text{Sr}_{\text{standard}} = 0.1194$ as the internal standard.

4. Results

Major elements, trace elements, and CIPW norm mineral calculation results of the Yangzhuang granite porphyry as well as the RCAG are given in Table 2. Data of the Yangzhuang granite porphyry from Zhang and Zhang (2014) are identical to ours, therefore, they will be used in combination with our data. The majority of the element contents in the RCAG are in good accordance with the Yangzhuang granite porphyry. However, significant differences in several elements are noticed.

4.1. Major element compositions

The Yangzhuang granite porphyry has higher SiO_2 contents (75.2–78.3 wt.%) and similar $\text{Na}_2\text{O} + \text{K}_2\text{O}$ contents (7.83–9.03 wt.%) compared with the RCAG (SiO_2 : 74.1–76.6 wt.%; $\text{Na}_2\text{O} + \text{K}_2\text{O}$: 7.60–9.08 wt.%). The CaO contents range from 0.29 wt.% to 1.00 wt.% and the Al_2O_3 contents range from 12.3 wt.% to 13.1 wt.%. Both of them are comparable to the RCAG (0.14 wt.%–1.07 wt.% and 11.0 wt.%–13.3 wt.%, respectively). Data of the Yangzhuang granite porphyry and the RCAG plot in the “subalkalic granite” field in the $(\text{K}_2\text{O} + \text{Na}_2\text{O})$ vs. SiO_2 diagram (Fig. 4a) and the “Alkaline” field in the SiO_2 vs. A.R. diagram (Fig. 4b). The aluminum-to-alkali (A/NK) ratios of all the studied granites range from 0.99 to 1.15, and the aluminum saturation indexes (A/CNK) range from 0.93 to 1.08, showing a meta-aluminous to weakly peraluminous property (Fig. 4c).

CIPW norm mineral calculation of the Yangzhuang granite porphyry and the RCAG demonstrate the dominant contents of quartz (Qz), albite (Ab), and orthoclase (Or) relative to anorthite (An). All the data plot into the field of alkali-feldspar granite in the quartz–alkaline feldspar-plagioclase feldspar (QAP) diagram (Fig. 4d). Differentiation Index (DI) of the Yangzhuang granite porphyry is much higher than the RCAG, implying a stronger degree of differentiation.

4.2. Trace element compositions

The ΣREE of the Yangzhuang granite porphyry range from 86.7 ppm to 136 ppm, and the LREE lean to the right and the HREE lean to the left with pronounced negative Eu anomalies ($\delta\text{Eu} = 0.07$ –0.11). The ΣREE of the RCAG vary from 122 to 330 ppm, and perform a right leaning feature with obvious negative Eu anomalies ($\delta\text{Eu} = 0.06$ –0.41) (Fig. 4e).

In the primitive mantle-normalized spider diagram (Fig. 4f), the Yangzhuang granite porphyry is in good accordance with the RCAG. However, significant enrichment of Th, U, Nb, Ta and depletion of Ba, Sr, Eu, and Ti should be cautiously explained. Especially, the Nb, Ta

Table 2

Major elements (in wt. %), trace elements (in ppm) and CIPW results of the Yangzhuang granite porphyry and the RCAG.

Sample	YZ-1	YZ-2	YZ-3	YZ-4	YZ-5	YZ-6	YZ-7	YZ-8	YZ-9	BYH-1	BYH-11	BYH-12	BYH-13	BYH-14	BYH-15	KM	MG	HONG	AK	Hatu
Yangzhuang granite porphyry										Yangzhuang granite porphyry*					Regional coeval A-type granites**					
SiO ₂	77.17	75.83	75.66	76.15	76.95	76.68	76.36	75.15	76.43	76.50	76.90	78.30	76.34	77.99	77.01	74.40	74.42	74.28	74.10	76.60
Al ₂ O ₃	12.84	12.50	12.80	12.88	13.08	12.82	12.80	12.90	12.34	13.14	12.52	12.90	12.82	12.75	12.42	12.38	13.04	13.00	13.34	11.00
Fe ₂ O ₃	0.76	0.63	0.60	0.63	0.26	0.58	0.61	0.57	0.45	0.96	0.97	0.89	1.11	1.07	1.11	2.27	1.81	2.43	1.77	2.14
FeO	0.20	0.21	0.20	0.23	0.27	0.28	0.27	0.01	0.34	—	—	—	—	—	—	—	—	—	—	—
CaO	0.54	0.45	0.63	0.41	0.35	0.38	0.78	1.00	0.43	0.34	0.30	0.39	0.29	0.32	0.33	1.07	0.97	0.76	0.75	0.45
MgO	0.05	0.01	0.04	0.09	0.01	0.12	0.02	0.10	0.08	0.01	0.03	0.02	0.03	0.01	0.01	0.27	0.19	0.24	0.20	0.11
K ₂ O	3.02	4.22	4.06	3.87	4.04	4.00	3.27	3.30	3.25	4.17	4.02	3.61	4.48	4.05	4.24	3.77	4.69	4.01	4.86	3.98
Na ₂ O	4.81	4.81	4.71	4.99	4.79	4.90	4.76	4.94	5.43	4.68	4.07	4.43	4.11	4.35	4.14	4.26	4.06	4.60	4.22	3.62
TiO ₂	0.06	0.05	0.06	0.06	0.07	0.06	0.05	0.04	0.05	0.06	0.07	0.07	0.08	0.09	0.09	0.22	0.21	0.22	0.19	0.17
MnO	0.11	0.09	0.09	0.08	0.02	0.14	0.04	0.79	0.09	0.08	0.07	0.05	0.10	0.10	0.14	0.05	0.04	0.06	0.03	0.05
P ₂ O ₅	0.01	0.01	0.01	0.01	0.01	0.01	0.01	0.01	0.01	—	—	—	—	—	—	0.06	0.04	0.06	0.05	0.04
LOI	0.72	0.52	0.86	0.47	0.43	0.50	0.76	1.00	0.54	0.29	0.37	0.45	0.44	0.36	0.42	0.64	0.34	0.40	0.34	—
F	0.24	0.22	0.25	0.20	0.20	0.16	0.37	0.50	0.03	0.23	0.17	0.21	0.18	—	—	—	—	—	—	—
Total	100.53	99.55	99.97	100.07	100.48	100.63	100.10	100.31	99.47	100.46	99.49	101.32	99.98	101.08	99.91	99.35	99.69	99.96	99.74	98.20
Mg#	0.09	0.02	0.09	0.17	0.03	0.21	0.04	0.26	0.16	0.89	2.65	1.93	2.32	0.80	0.77	0.17	0.16	0.15	0.15	0.09
A.R.	3.82	5.61	4.76	5.00	4.84	5.14	3.89	3.91	5.24	4.82	4.42	4.06	4.80	4.60	4.84	4.25	4.54	4.40	4.76	4.93
La	23.10	20.80	21.30	24.40	28.30	23.70	19.70	24.30	21.70	18.40	20.80	20.00	21.50	20.80	27.40	20.43	27.06	25.82	25.24	63.10
Ce	39.80	29.50	37.50	39.80	44.50	36.20	39.70	45.60	41.10	42.22	44.86	39.31	40.81	43.45	57.82	47.63	61.42	57.58	58.89	139.00
Pr	3.97	3.42	3.15	3.94	4.82	4.17	3.32	4.00	3.58	3.71	3.84	3.40	3.85	4.07	5.39	6.18	7.77	8.54	8.12	18.50
Nd	10.80	8.77	8.19	10.50	13.50	11.60	8.68	10.70	9.71	10.00	10.10	8.45	9.84	11.10	15.80	23.50	30.94	32.28	34.22	65.70
Sm	2.36	1.89	1.40	1.94	2.54	2.62	1.66	2.10	1.91	1.97	1.96	1.53	1.90	2.29	3.45	5.13	6.57	7.15	8.04	11.80
Eu	0.07	0.05	0.05	0.07	0.08	0.07	0.05	0.05	0.05	0.06	0.05	0.04	0.05	0.07	0.11	0.62	0.85	0.56	0.41	0.21
Gd	2.65	2.19	1.76	2.12	2.78	2.89	1.96	2.50	2.31	2.42	2.31	1.81	1.93	2.48	3.40	4.31	6.16	5.87	7.33	9.09
Tb	0.57	0.51	0.35	0.45	0.50	0.59	0.41	0.54	0.50	0.55	0.52	0.46	0.48	0.57	0.79	0.73	1.06	1.05	1.31	1.40
Dy	4.87	4.55	2.90	4.01	4.06	5.07	3.73	4.35	4.38	4.36	4.01	3.78	3.77	4.30	5.65	5.66	7.19	8.14	9.45	10.10
Ho	1.23	1.21	0.81	1.07	1.05	1.31	1.05	1.13	1.22	1.30	1.19	1.19	1.12	1.20	1.51	1.13	1.46	1.65	1.91	1.93
Er	4.84	4.71	3.30	4.18	3.99	4.85	4.06	4.23	4.64	4.72	4.43	4.65	4.20	4.38	5.21	2.92	4.01	4.35	5.18	4.67
Tm	0.89	0.88	0.65	0.83	0.79	0.91	0.79	0.82	0.90	0.93	0.88	0.91	0.82	0.85	0.95	0.44	0.62	0.71	0.80	0.65
Yb	7.07	7.06	5.57	6.83	6.39	6.92	6.46	6.60	7.28	7.32	7.08	7.16	6.39	6.76	7.03	2.81	3.93	4.31	4.90	3.77
Y	42.50	39.60	29.50	37.10	35.40	40.50	34.30	37.90	40.20	47.70	44.80	48.30	39.70	43.80	50.90	32.93	40.95	50.56	54.96	54.50
Lu	1.16	1.19	0.93	1.17	1.10	1.10	1.04	1.08	1.23	1.18	1.20	1.23	1.07	1.09	1.13	0.40	0.59	0.58	0.69	0.48
Ba	32.10	7.50	41.40	23.80	7.15	11.90	42.20	214.00	44.70	13.40	43.00	16.40	68.70	20.10	36.10	605.00	612.73	347.60	325.40	134.00
Cr	3.48	0.83	5.97	2.44	1.90	9.56	5.44	2.10	3.32	277.00	504.00	492.00	543.00	407.00	409.00	8.88	7.44	6.61	12.08	6.30
Zr	190.20	215.10	200.10	206.00	213.10	211.20	203.20	202.90	207.30	162.00	184.00	171.00	177.00	182.00	181.00	216.70	242.20	153.00	232.40	273.00
Hf	11.70	10.40	10.70	10.20	10.80	9.93	10.40	10.70	10.80	8.98	9.75	9.10	9.49	8.66	8.57	7.42	7.34	4.87	7.50	8.72
Nb	93.60	87.20	84.40	92.80	90.60	86.60	100.00	81.90	95.80	101.00	118.00	95.30	121.00	106.00	107.00	10.20	8.75	8.77	8.88	10.40
Ni	1.53	0.29	1.43	0.85	0.49	2.77	1.90	0.92	1.11	166.00	289.00	274.00	308.00	227.00	236.00	3.33	2.51	3.41	3.11	3.82
Rb	185.00	297.00	271.00	280.00	269.00	237.00	144.00	200.00	171.00	218.00	194.00	171.00	209.00	185.00	184.00	98.73	123.84	107.16	124.30	121.00
Sc	2.74	1.87	2.53	2.44	3.12	3.20	2.29	4.67	1.99	3.42	3.95	4.15	3.62	3.13	2.45	3.76	5.79	5.53	3.68	2.85
Sr	24.80	5.12	24.30	13.00	11.20	14.60	10.80	226.00	17.50	5.96	15.20	16.60	20.90	16.10	37.40	54.67	118.45	103.80	56.30	23.00
Ga	22.60	21.90	21.90	22.60	23.70	22.70	23.40	26.20	22.00	27.9	25.9	25.8	25.6	26.3	26.1	—	—	—	—	—
Pb	92.20	31.60	29.20	27.90	30.20	11.10	66.50	128.00	22.20	46.68	43.53	64.50	85.11	37.22	59.89	—	—	—	—	—
Ta	8.04	7.77	8.32	8.36	7.91	7.62	8.53	5.71	8.34	7.84	9.41	8.41	8.85	7.79	7.83	1.03	0.61	0.75	0.76	0.57
Th	30.40	20.80	24.60	28.90	28.80	23.80	25.30	28.40	27.20	26.40	31.40	28.60	33.90	25.70	26.50	13.71	10.16	14.14	7.99	9.93
U	6.46	5.12	3.46	4.40	5.74	4.59	5.37	76.40	6.90	5.95	6.82	5.61	6.63	6.37	5.46	4.62	2.05	1.90	1.81	1.69
Be	6.18	8.97	5.78	6.47	7.59	10.20	13.20	71.70	24.70	9.73	10.73	4.17	9.67	10.35	7.82	—	—	—	—	—
Q	37.72	32.55	32.69	32.93	34.63	32.40	36.21	34.85	32.80	33.10	37.86	38.05	35.18	36.06	35.95	32.92	30.67	30.07	29.09	39.55
An	0.00	0.00	0.19	0.00	0.00	0.09	0.00	0.00	0.00	0.01	0.28	0.44	0.13	1.59	1.67	3.57	3.51	2.99	3.10	2.05
Ab	40.22	39.94	40.14	41.15	38.71	41.37	40.43	39.21	45.66	39.55	34.76	37.18	34.95	36.56	35.23	36.56	34.58	39.11	35.95	31.24
Or	17.85	25.14	24.17	22.92	23.82	23.59	19.42	19.55	19.35	24.61	23.98	21.16	26.61	23.77	25.20	22.58	27.89	23.82	28.90	23.99
Di	95.79	97.63	97.00	97.00	97.16	97.36	96.06	93.61	97.81	97.26	96.60	96.39	96.74	96.38	92.06	93.14	93.00	93.94	94.78	—
H ₂ O	4.85	4.69	4.64	4.66	4.75	4.68	4.77	4.55	4.80	4.65	4.89	4.91	4.71	4.83	4.83	4.42	4.30	4.25	4.23	4.97
A/CNK	1.05	0.94	0.96	0.98	1.01	0.98	1.00	0.95	0.93	1.02</										

content of the Yangzhuang granite porphyry is nearly 10 times that of the RCAG (Table 2).

4.3. Sm–Nd–Rb–Sr–Pb isotopes

Measured and initial (back-calculated to 310 Ma) Sm–Nd–Rb–Sr–Pb isotopes of the Yangzhuang granite porphyry and the RCAG are reported in Tables 3 and 4. $^{87}\text{Sr}/^{86}\text{Sr}_i$ of the Yangzhuang granite porphyry range

widely from 0.70544 to 0.74688, and ϵNd (t) vary from 4.1 to 5.9. $^{87}\text{Sr}/^{86}\text{Sr}_i$ of the RCAG have a narrower range of 0.7024 to 0.7045 and the ϵNd (t) (7.1–8.9) are much higher than the Yangzhuang granite porphyry. $T_{2\text{DM}}$ of Nd isotopes of the Yangzhuang granite porphyry is much older than that of the RCAG.

For the Yangzhuang granite porphyry, the initial Pb isotopic ratio $^{206}\text{Pb}/^{204}\text{Pb}_i$ ranges from 18.104 to 18.707, $^{207}\text{Pb}/^{204}\text{Pb}_i$ ranges from 15.503 to 15.555, and $^{208}\text{Pb}/^{204}\text{Pb}_i$ ranges from 37.625 to 38.200.

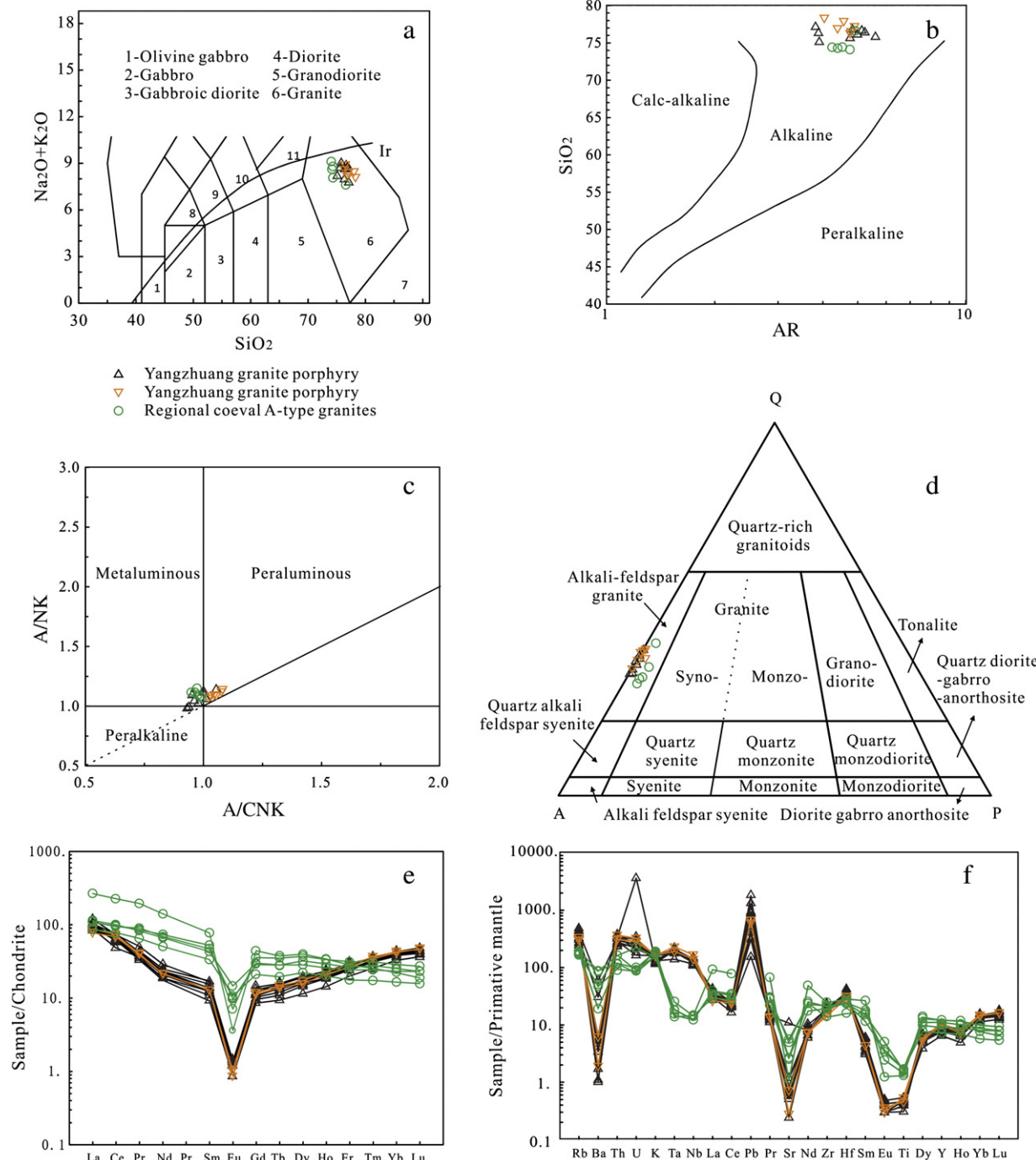


Fig. 4. (a) SiO_2 vs. $(\text{Na}_2\text{O} + \text{K}_2\text{O})$ diagram (Middlemost, 1994). The alkaline and subalkaline division is after Irvine and Baragar (1971); (b) $\text{A.R.} = (\text{Al}_2\text{O}_3 + \text{CaO} + \text{Na}_2\text{O} + \text{K}_2\text{O})/(\text{Al}_2\text{O}_3 + \text{CaO} - \text{Na}_2\text{O} - \text{K}_2\text{O})$; (c) QAP diagram of the Yangzhuang granite porphyry; (d) A/NK vs. A/CNK diagram of the Yangzhuang granite porphyry; (e) Rare earth element pattern diagram of the Yangzhuang granite porphyry; (f) Spider trace element variation diagrams of the Yangzhuang granite porphyry. Chondrite and N-MORB normalizing values are after Sun and McDonough (1989).

Data of gray triangles are from Zhang and Zhang (2014).

Table 3

Sm–Nd–Rb–Sr isotope composition of the Yangzhuang granite porphyry and the RCAG.

Sample	Rock type	Rb (ppm)	Sr (ppm)	$^{87}\text{Rb}/^{86}\text{Sr}_{\text{m}}$	$^{87}\text{Sr}/^{86}\text{Sr}_{\text{m}}$	Sm (ppm)	Nd (ppm)	$^{147}\text{Sm}/^{144}\text{Nd}_{\text{m}}$	$^{143}\text{Nd}/^{144}\text{Nd}_{\text{m}}$	$^{87}\text{Sr}/^{86}\text{Sr}_{\text{i}}$	ϵNd (<i>t</i>)	T _{2DM} (Ma)
YZ-1	Granite porphyry	145	28.7	14.6393	0.774825	2.51	12.8	0.1182	0.512753	0.71041	5.3	636
YZ-2	Granite porphyry	214	8.26	74.9998	1.121285	2.33	11.8	0.1197	0.512747	–	5.2	650
YZ-3	Granite porphyry	204	28.4	20.7906	0.811015	1.96	10.9	0.1084	0.512762	0.71953	5.9	590
YZ-9	Granite porphyry	143	21.7	19.0954	0.789464	2.13	11.2	0.1146	0.512774	0.70544	5.9	591
BYH-12*	Granite porphyry	–	–	0.87633	–	–	–	–	0.51274	0.74663	5.3	–
BYH-13*	Granite porphyry	–	–	0.86381	–	–	–	–	0.51274	0.73791	5.1	–
BYH-14*	Granite porphyry	–	–	0.89155	–	–	–	–	0.51275	0.74688	4.9	–
BYH-15*	Granite porphyry	–	–	0.77625	–	–	–	–	0.51272	0.71431	4.1	–
KM9918-3**	Alkali-feldspar granite	118.1	144	2.38	0.71389	5.43	25.6	0.13	0.512957	0.7036	8.9	342
MG136-1**	Alkali-feldspar granite	71.3	336	0.61	0.70646	9.96	39.3	0.15	0.512954	0.7038	7.9	428
HONG1**	Alkali-feldspar granite	85.3	72	3.45	0.71829	7.53	45.7	0.1	0.512838	0.7033	7.7	441
AK154-2**	Alkali-feldspar granite	99.8	45	6.41	0.73156	3.77	19.9	0.11	0.512911	0.7037	8.5	374
Hatu**	Alkali-feldspar granite	113.8	33	9.98	0.74575	10.29	45.3	0.14	0.512935	0.7024	8.1	407
MG4**	Alkali-feldspar granite	108.4	75	4.21	0.72232	8.17	34.9	0.14	0.512893	0.7044	7.1	488
MG16**	Alkali-feldspar granite	131.8	61	6.32	0.73102	7.88	42.4	0.11	0.512903	0.7041	8.5	378
MG19**	Alkali-feldspar granite	115.1	54	6.13	0.73064	8.42	36.6	0.14	0.512913	0.7045	7.6	448
MG24**	Alkali-feldspar granite	107.6	85	3.66	0.71906	6.63	30.5	0.13	0.51289	0.7034	7.5	460
MG26**	Alkali-feldspar granite	130.1	128	2.94	0.71648	5.83	28.1	0.13	0.512911	0.7039	8.1	408

Subscript “m” refers to measure, and “i” refers to initial.

Data with * are from Zhang and Zhang (2014).

Data with ** are the average of Karamay, Hongshan, Akbastao, and Hatu from Chen and Arakawa (2005), and Geng et al. (2009).

5. Discussion

5.1. The genesis of the Yangzhuang granite porphyry

Feldspar in the phenocryst and the matrix of the Yangzhuang granite porphyry are dominantly alkali-feldspar. There is barely any anorthite as indicated by CIPW norm mineral calculations (Table 2). The Yangzhuang granite porphyry is classified as A-type granite because of: (1) the relatively high content of SiO₂, Na₂O + K₂O, Fe/Mg, F, Nb, Ga, Sn, Y, and rare earth elements and low content of CaO, Ba, Sr, P, and Ti; (2) the significantly negative Eu anomaly; (3) 10000 Ga/Al = 3.23–3.84, evidently greater than the lower limit of A-type granite, i.e., 2.6 (Whalen et al., 1987).

The Yangzhuang granite porphyry plots in the A-type granite field in various discrimination diagrams (Fig. 5a, b). A previous study indicates that the RCAG including Hongshan, Karamay, Tiechanggou, Hatu, Akbastao, Miaoergou, Kulumusu, and Sailleke are all A₂-type granites (Geng et al., 2009; Su and Tang, 2005; Tang et al., 2010a). However, the Yangzhuang granite porphyry falls in the A₁-type granite field (Fig. 5c, d) owing to the enriched Nb content (the RCAG are not shown in Fig. 5a, c due to the absence of Ga content in the references).

The high Differentiation Index (DI) together with the strong depletion of Eu, Ba, and Sr of the Yangzhuang granite porphyry implies a considerable fractional crystallization. Depleted Eu and Sr can be attributed to the fractionation of plagioclase, however, the intensively depleted Ba indicates the fractionation of K-feldspar as well (Eby, 1990; Han et al., 1997).

Granitoids in West Junggar are universally featured with positive ϵNd (*t*) values varying from +2.6 to +9 (Han et al., 1998), and the Yangzhuang granite porphyry is no exception. The positive ϵNd (*t*) value of granites in West Junggar indicates that the magma originated from juvenile continental crust (Chen and Arakawa, 2005) or metasomatized depleted mantle with some crustal contamination (Han et al., 1997). The ϵNd (*t*) value of the Yangzhuang granite porphyry

(4.1–5.9) is lower than the RCAG (7.1–8.9), and the T_{2DM} is correspondingly older (Fig. 6). Han et al. (1998) considered crustal contamination to be the main cause of the low ϵNd (*t*) value and relatively old Nd model age in West Junggar. The relatively lower ϵNd (*t*) value (0.19–1.88) and older Nd model ages (600–803 Ma) of the Xuemisitan volcanic rocks make it possible to decrease the ϵNd (*t*) value of the Yangzhuang granite porphyry by crustal contamination (Shen et al., 2012). The smaller size of the Yangzhuang granite porphyry is more likely to have gone through more crustal contamination than the RCAG.

The initial $^{87}\text{Sr}/^{86}\text{Sr}$ ratio of the Yangzhuang granite porphyry vary over an extremely wide range (0.7054–0.74688), far wider than the RCAG (0.7024–0.7045). Previous research has demonstrated that injection of oceanic sediment and seawater will lead to a rise in the magma $^{87}\text{Sr}/^{86}\text{Sr}$ ratio (Harris et al., 1982). However, the high $^{87}\text{Sr}/^{86}\text{Sr}$ isotope endmember will gradually be homogenized after entering the magma chamber, which fails to explain the extremely wide span of initial $^{87}\text{Sr}/^{86}\text{Sr}$ ratio of the Yangzhuang granite porphyry. Heterogeneous crustal contamination is preferred to interpret the formation of the large $^{87}\text{Sr}/^{86}\text{Sr}$ isotope variation. In addition, the Rb–Sr system is more easily influenced than the Sm–Nd system during the hydrothermal process. Therefore, the probability of Be–U mineralization leading to variation in Sr isotope cannot be excluded.

The μ value ($^{238}\text{U}/^{204}\text{Pb} = 9.32\text{--}9.37$) of the Yangzhuang granite porphyry is lower than the average crust value (9.74). The typical crust-derived granite is mostly located in the upper crust or the lower crust region on the Pb isotope tectonic evolution diagram (Fig. 7) (Zhang et al., 1993). However, the Pb isotope of the Yangzhuang granite porphyry is distributed between the mantle evolution line and the upper crust evolution line showing its affinity to a mantle source.

5.2. Decouple of Nb–Ta, Zr–Hf, and Ti

High-field-strength elements Nb–Ta (HFSE⁵⁺), Zr–Hf (HFSE⁴⁺), and Ti share similar crystal–chemical properties, and therefore, are not

Table 4

Pb isotope composition of the Yangzhuang granite porphyry.

Samples	Rock type	$^{206}\text{Pb}/^{204}\text{Pb}$	2σ	$^{207}\text{Pb}/^{204}\text{Pb}$	2σ	$^{208}\text{Pb}/^{204}\text{Pb}$	2σ	t (Ma)	$^{206}\text{Pb}/^{204}\text{Pb}_i$	$^{207}\text{Pb}/^{204}\text{Pb}_i$	$^{208}\text{Pb}/^{204}\text{Pb}_i$	μ	Th/U
YZ-1	Granite porphyry	18.354	0.002	15.523	0.002	38.059	0.004	310	18.104	15.510	37.687	9.32	3.59
YZ-2	Granite porphyry	19.300	0.004	15.586	0.003	38.961	0.008	310	18.707	15.555	38.200	9.37	3.51
YZ-3	Granite porphyry	18.731	0.001	15.547	0.001	38.587	0.003	310	18.303	15.525	37.625	9.33	3.63
YZ-9	Granite porphyry	19.365	0.001	15.563	0.001	39.111	0.003	310	18.224	15.503	37.690	9.32	3.53

Subscript “m” refers to measure, and “i” refers to initial.

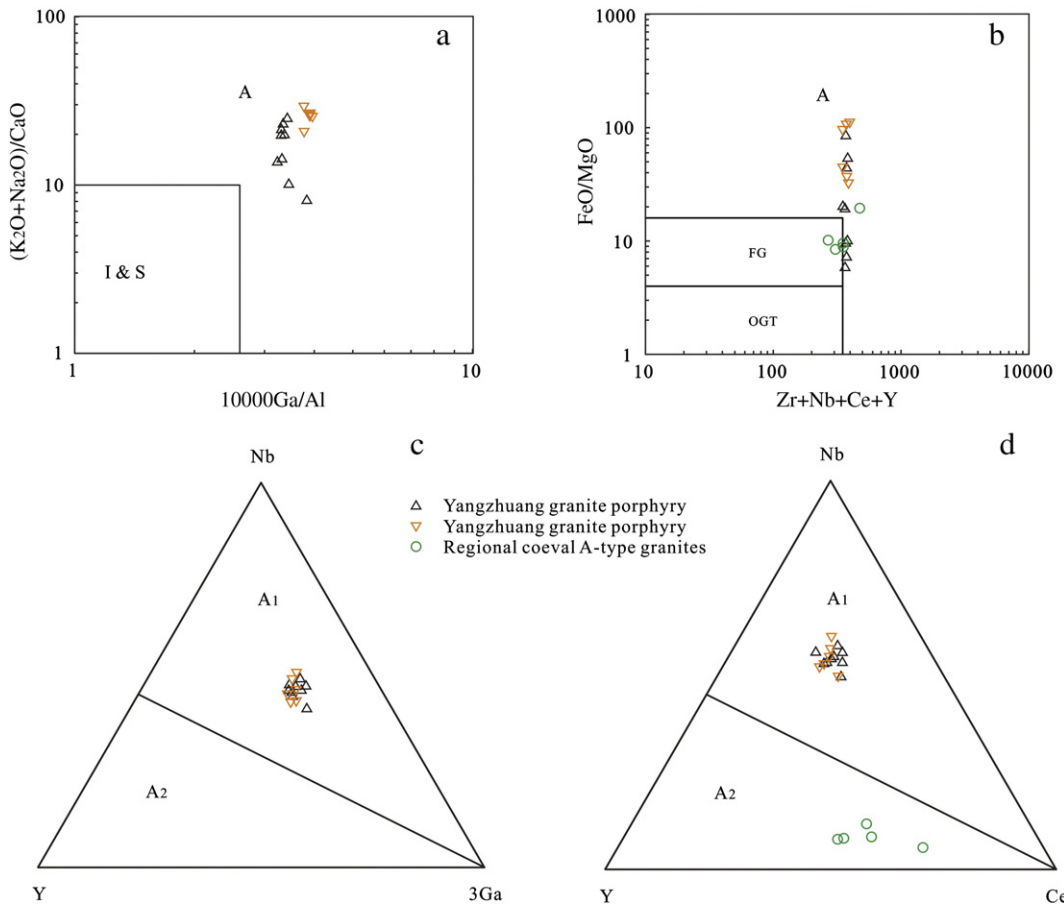


Fig. 5. Chemical classification diagrams of A-type granite. (a) $(\text{K}_2\text{O} + \text{Na}_2\text{O})/\text{CaO}$ vs. 10000 Ga/Al diagram; (b) FeO/MgO vs. $(\text{Zr} + \text{Nb} + \text{Ce} + \text{Y})$ diagram; (c) $\text{Nb}-\text{Y}-3\text{Ga}$ diagram; (f) $\text{Nb}-\text{Y}-\text{Ce}$ diagram (a, b after Whalen et al., 1987; c, d after Eby, 1992).

expected to fractionate greatly during the partial melting and crystallization processes (Sun and McDonough, 1989; Tiepolo et al., 2001). The Yangzhuang granite porphyry is intensively enriched with Nb, Ta and more depleted with Ti compared to the RCAG, however, the contents of Zr, and Hf are similar to that of the RCAG (Fig. 4f). Therefore, Nb-Ta, Zr-Hf and Ti were decoupled during the formation of the Yangzhuang granite porphyry.

Owing to the extremely high partition coefficients of Nb and Ta in rutile and ilmenite (Ionov and Hofmann, 1995), the Nb-Ta-Ti depletion

in island-arc magmatic rock is mostly interpreted as a remnant of provenance minerals such as rutile and ilmenite. Melting of provenance rutile and ilmenite can cause Nb-Ta enrichment in magma, but it fails to explain the coexistence of strong enrichment of Nb and Ta and intense depletion of Ti in the Yangzhuang granite porphyry.

The mineralization fluid temperature of the Baiyanghe Be-U deposit is about 120 °C–150 °C according to the fluid inclusion study of fluorite

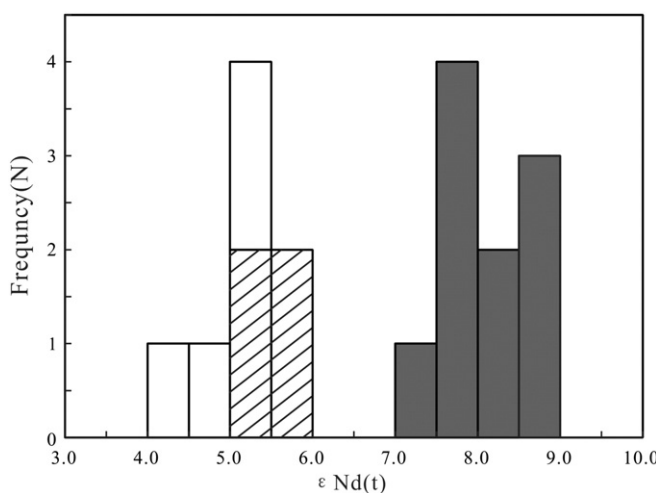


Fig. 6. ϵ_{Nd} (t) histogram of the Yangzhuang granite porphyry and RCAG (blank and hatched refer to Yangzhuang granite porphyry. Gray refers to the RCAG).

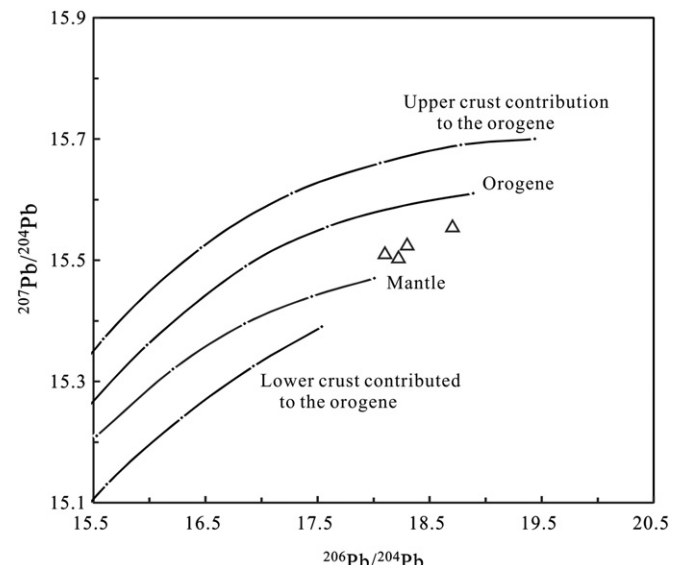


Fig. 7. Pb isotope tectonic evolution diagram of the Yangzhuang granite porphyry.

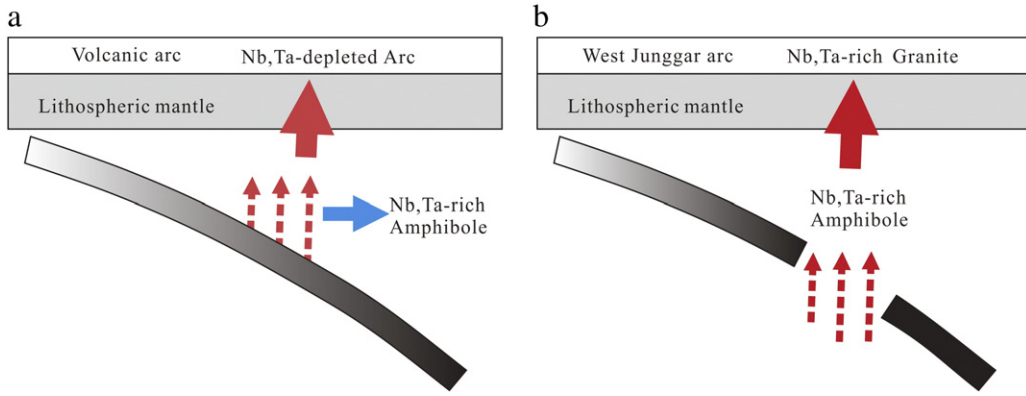


Fig. 8. Formation and decomposition model of the Nb and Ta-rich amphibole in the mantle wedge.

(Mao et al., 2013). It is impossible for such low-temperature fluid alteration to cause differentiation among high-field-strength elements (Ionov and Hofmann, 1995). The average Nb content in the earth's crust is merely 19 ppm (Li, 1976), and the average Nb content in the Xuemisitan volcanic belt is 19.5 ppm (Shen et al., 2012). Therefore, the possibility of crustal contamination causing Nb-Ta enrichment in the Yangzhuang granite porphyry can be excluded.

Hofmann (1988) firstly proposed that amphibole, a most common hydrous mineral in the upper mantle, can be an important host for Nb and Ta. Ionov and Hofmann (1995) reported that the Nb and Ta contents of the vein amphibole (and mica) of mantle xenolith had been enriched to a magnitude 50–200 times that of the primitive mantle. Hence, they proposed a metasomatic model for the formation of Nb and Ta enriched amphibole (and mica) in the mantle wedge. When the fluids generated by dehydration of the subducted slab ascend through the mantle wedge, highly incompatible elements including Nb and Ta are transferred into the mantle wedge by the precipitation of amphibole (Fig. 8a).

Experimental investigations reveal that Nb becomes compatible, whereas Zr remains incompatible, in amphibole crystallized in Ti-poor systems in the mantle wedge. With $D_{Nb}^{Amph/L}$ values up to 1.8, Nb incorporation is strongly favored in low-Mg-number amphiboles. Therefore, crystallization of low-Mg-number amphibole in Ti-depleted system from silica-rich aqueous fluids (water-rich silicic melts) released from the subducted slab will lead to the decoupling of Nb (Ta), Zr (Hf), and Ti (Tiepolo et al., 2001, 2007). It is inferred that melting of the above Nb- and Ta-rich and Ti-poor amphibole under particular circumstances, e.g. ridge subduction (Fig. 8b), can carry its trace element feature to the Yangzhuang granite porphyry.

5.3. Tectonic setting

The tectonic setting in the Late Carboniferous–Early Permian in West Junggar is still under debate (Chen and Arakawa, 2005; Chen et al., 2010; Choulet et al., 2011, 2012a, 2012b; Geng et al., 2009; Han et al., 1997; Shen et al., 2012). The post-collisional model is now highly challenged because of the lack of structural or metamorphic evidence for a collisional event in the Late Carboniferous (Feng et al., 1989) and the existence of an oceanic basin (Choulet et al., 2011; Wang, 2006; Wang et al., 2007a). Zhang and Zhang (2014) attributed the formation of the Yangzhuang granite porphyry to the southward subduction of the Irtysh–Zaysan oceanic lithosphere beneath the Zharma–Saur arc because the Yangzhuang granite porphyry and the controlling fault show a nearly E–W trend, which is compatible with the N–S extensional environment of the back-arc basin behind the Zharma–Saur arc. However, the Zharma–Saur suture zone was already closed in the late Carboniferous due to the oldest stitching pluton dated at 307 Ma (Chen et al., 2010; Kuibida et al., 2009), so the existence of a back-arc extensional basin is highly doubted. Late Paleozoic ocean in West Junggar became smaller with residual nature due to the large scale accretion of continental crust before Silurian, therefore, the back-arc basin might be absent during the closure of this residual ocean (Zhao and He, 2013). Moreover, various tectonic settings, e.g. ridge subduction, can provide extensional environments.

Sedimentary and paleogeographic analysis implies that there was a NE–SW stretching Carboniferous Junggar Ocean parallel to the Karamay arc in Late Carboniferous–Early Permian (Tang et al., 2010a; Wang, 2006). Northwestward subduction of the Junggar oceanic lithosphere beneath the Karamay arc is more likely to form such a NE–SW stretching

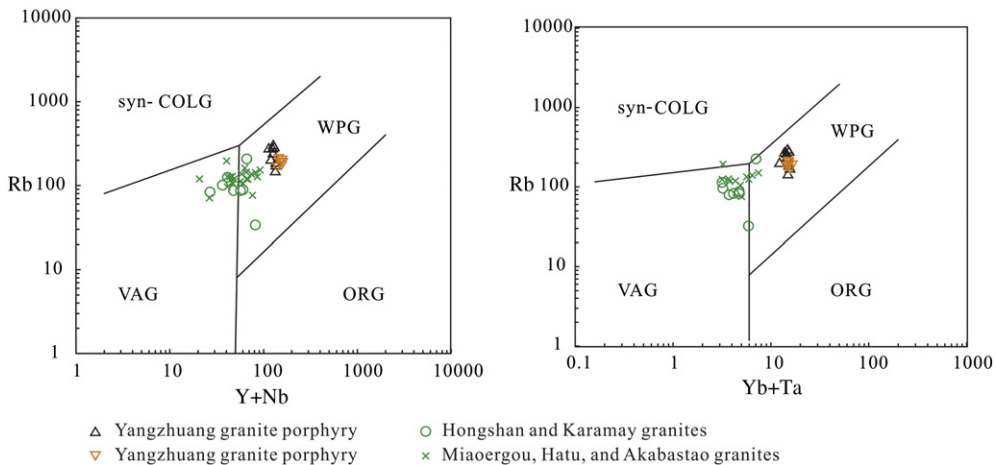


Fig. 9. Trace element diagrams for tectonic discrimination (after Pearce et al., 1984). (a) Rb vs. (Y + Nb); (b) Rb vs. (Yb + Ta). Abbreviations: VAG (volcanic-arc granites); syn-COLG (syn-collisional granites); WPG (within-plate granites); ORG (ocean-ridge granites).

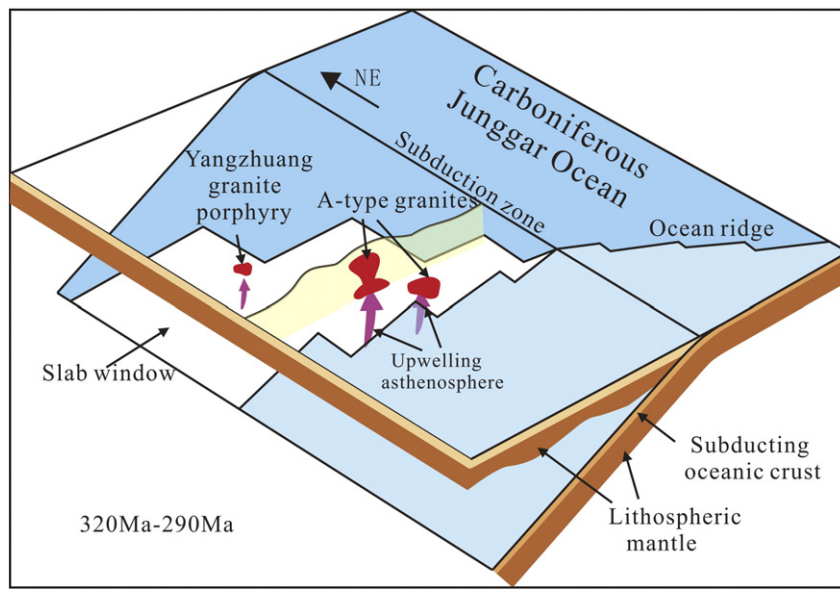


Fig. 10. Proposed tectonic model for the West Junggar granites in the Late Carboniferous–Early Permian. Modified after Tang et al. (2010a, 2010b).

ocean. Additionally, the adakite and the Nb-enriched basalt to the southwest of the West Junggar and the tholeiitic basaltic magmatism to the east of the Junggar basin are all formed in a Late Carboniferous subduction setting (Long et al., 2006; Wang et al., 2007b; Zhang et al., 2011a).

Black circles plotted in the VAG (volcanic-arc granites) field (Fig. 9) referring to the Hongshan and Karamay granites are close to the subduction zone implied by Geng et al. (2009) and Tang et al. (2010a). Black crosses referring to the Miaoergou, Hatu, and Akbastao granites that are further to the subduction zone are located at the intersection area of VAG and WPG (within-plate granites). The Yangzhuang granite porphyry represented by black and gray triangles is totally in the WPG field. Therefore, the geochemical transformation from VAG to WPG supports a northwestward subduction model.

5.4. Ridge subduction

Various volcanic and intrusive rocks in West Junggar formed in the Late Carboniferous–Early Permian are derived from a mantle magmatic source (Chen and Arakawa, 2005; Chen and Jahn, 2004; Geng et al., 2009, 2011; Han et al., 2006; Tang et al., 2010a, 2010b; Yin et al., 2010; Zhang et al., 2011a, 2011b). The dioritic rocks with adakitic characteristics in West Junggar were formed by partial melting of an oceanic slab which required high temperature (Geng et al., 2009). The ~320 Ma sanukite-like high-Mg dikes in the West Junggar imply not only an extensional setting, but also a high temperature geothermal gradient (Yin et al., 2010). Tang et al. (2012) reported a ~315 Ma MORB-like tholeiites in Hatu which was originated from a mixed mantle source consisting of subducted depleted oceanic lithosphere and enriched upwelling asthenospheric mantle. Volcanic rocks in the Maliya ophiolitic mélange formed in the Late Carboniferous show similar characteristic to that of the rocks formed during ridge subduction in Chile (Zhang et al., 2010). All these evidences point to the ridge subduction model proposed by Geng et al. (2009). The paleostress inversion and structural analyses indicate that the NW/SE trending dioritic dike swarm was derived from magma upwelling with a NW–SE trend that resulted from ridge subduction (Ma et al., 2012).

Therefore, the ridge subduction model is favored for the formation of the Nb- and Ta-rich and Ti poor Yangzhuang granite porphyry. As is

located in the Xuemisitan volcanic belt, the Baiyanghe area must have gone through two stages of southward subduction during the formation of the Xuemisitan volcanic belt and the Zharma-Saur arc (Shen et al., 2012). The mantle wedge, therefore, was extensively metasomatized by dehydration of the subducting slab. Nb and Ta are strongly enriched in the mantle wedge where Nb and Ta rich and Ti-poor amphibole was crystallized during the long-term metasomatism (Fig. 8a). A northwestward subduction took place in the Late Carboniferous to intensify the metasomatism and the formation of amphibole. The specific location of the Yangzhuang granite porphyry suffered all three stages of subduction and thus the mantle wedge must have contained abundant Nb- and Ta-rich and Ti-poor amphibole.

As the ocean ridge subducted, upwelling asthenosphere through the slab window provided enhanced heat flux and triggered the magmatism (Geng et al., 2009). The abundant amphibole in the mantle wedge undoubtedly broke down to generate Nb- and Ta-rich and Ti-poor melt (Fig. 8b). Partial melting of the hot juvenile lower crust injected with such melt then produced the Nb- and Ta-rich and Ti-poor Yangzhuang granite porphyry (Fig. 10).

6. Conclusions

Based on the systematic comparison between the Yangzhuang granite porphyry and the RCAG by whole-rock geochemistry and Sr–Nd–Pb isotope studies in West Junggar, the following conclusions can be drawn:

- (1) Multi-stage of metasomatism may lead to the intensive enrichment of Nb and Ta in mantle wedge by precipitation of amphibole, and the enhanced heat flux can decompose the Nb- and Ta-rich amphibole to generate Nb and Ta-enriched melt under certain circumstances.
- (2) The Yangzhuang granite porphyry is intensively enriched with Nb and Ta and depleted with Ti relative to the RCAG. Therefore, the decomposition of the mantle wedge amphibole triggered by Late Carboniferous ridge subduction is attributed to the formation of the Nb- and Ta-rich Yangzhuang granite porphyry.
- (3) Sr–Nd–Pb isotope study reveals that the Yangzhuang granite porphyry has an origin of a juvenile lower crust and had gone through crustal contamination to some extent as well.

Acknowledgments

This study was financially supported by the One Hundred Person Project of the Chinese Academy of Sciences and a scientific project from China National Nuclear Corporation (CNNC). We are grateful to Dr. Nelson Eby, Dr. Flavien Choulet, Dr. Min Sun and the anonymous referees for their constructive reviews and significant help in improving the original manuscript. We are grateful to colleagues from the 216 team, CNNC, for their assistance during the field seasons.

References

- Bédard, J., 1990. Enclaves from the A-type granite of the Mégantic Complex, White Mountain Magma Series: clues to granite magmogenesis. *Journal of Geophysical Research* 95, 17797–17819.
- Bonin, B., 2007. A-type granites and related rocks: evolution of a concept, problems and prospects. *Lithos* 97, 1–29.
- Chen, B., Arakawa, Y., 2005. Elemental and Nd-Sr isotopic geochemistry of granitoids from the West Junggar foldbelt (NW China), with implications for Phanerozoic continental growth. *Geochimica et Cosmochimica Acta* 69, 1307–1320.
- Chen, B., Jahn, B., 2004. Genesis of post-collisional granitoids and basement nature of the Junggar Terrane, NW China: Nd-Sr isotope and trace element evidence. *Journal of Asian Earth Sciences* 23, 691–703.
- Chen, J.F., Han, B.F., Ji, J.Q., Zhang, L., Xu, Z., He, G.Q., Wang, T., 2010. Zircon U-Pb ages and tectonic implications of Paleozoic plutons in northern West Junggar, North Xinjiang, China. *Lithos* 115, 137–152.
- Choulet, F., Chen, Y., Wang, B., Faure, M., Cluzel, D., Charvet, J., Lin, W., Xu, B., 2011. Late Paleozoic paleogeographic reconstruction of Western Central Asia based upon paleomagnetic data and its geodynamic implications. *Journal of Asian Earth Sciences* 42, 867–884.
- Choulet, F., Faure, M., Cluzel, D., Chen, Y., Lin, W., Wang, B., 2012a. From oblique accretion to transpression in the evolution of the Altaiid collage: new insights from West Junggar, northwestern China. *Gondwana Research* 21, 530–547.
- Choulet, F., Faure, M., Cluzel, D., Chen, Y., Lin, W., Wang, B., Jahn, B.M., 2012b. Architecture and evolution of accretionary orogens in the Altaiids Collage: the early paleozoic West Junggar. *American Journal of Science* 312, 1098–1145.
- Clemens, J.D., Holloway, H.R., White, A.J.R., 1986. Origin of an A-type granite: experimental constraints. *American Mineralogist* 71, 317–324.
- Collins, W.J., Beams, S.D., White, A.J.R., Chappell, B.W., 1982. Nature and origin of A-Type granites with particular reference to Southeastern Australia. *Contributions to Mineralogy and Petrology* 80, 189–200.
- Didenko, A.N., Morozov, O.L., 1999. Geology and paleomagnetism of Middle–Upper Paleozoic rocks of the Saur Ridge. *Geotectonics* 4, 64–80 (in Russian with English abstract).
- Eby, G.N., 1990. The A-type granitoids: a review of their occurrence and chemical characteristics and speculations on their petrogenesis. *Lithos* 26, 115–134.
- Eby, G.N., 1992. Chemical subdivision of the A-type granitoids: petrogenetic and tectonic implications. *Geology* 20, 641–644.
- Feng, Y., Coleman, R.G., Tilton, G., Xiao, X., 1989. Tectonic evolution of the West Junggar region, Xinjiang, China. *Tectonics* 8, 729–752.
- Filippova, I.B., Bush, V.A., Didenko, A.N., 2001. Middle Paleozoic subduction belts: the leading factor in the formation of the Central Asian fold-and-thrust belt. *Russian Journal of Earth Sciences* 3, 405–426.
- Gao, S.L., He, Z.L., Zhou, Z.Y., 2006. Geochemical characteristics of the Karamay granitoids and their significance in West Junggar, Xinjiang. *Xinjiang Geology* 24, 125–130 (in Chinese with English abstract).
- Geng, H.Y., Sun, M., Yuan, C., Xiao, W.J., Xian, W.S., Zhao, G.C., Zhang, L.F., Wong, K., Wu, F.Y., 2009. Geochemical, Sr-Nd and zircon U-Pb-Hf isotopic studies of Late Carboniferous magmatism in the West Junggar, Xinjiang: implications for ridge subduction? *Chemical Geology* 266, 364–389.
- Geng, H.Y., Sun, M., Yuan, C., Zhao, G.C., Xiao, W.J., 2011. Geochemical and geochronological study of early Carboniferous volcanic rocks from the West Junggar: petrogenesis and tectonic implications. *Journal of Asian Earth Sciences* 42, 854–866.
- Han, B.F., Wang, S.G., Jahn, B., Hong, D.W., Kagami, H., Sun, Y.L., 1997. Depleted-mantle source for the Ulungur River A-type granites from North Xinjiang, China: geochemistry and Nd-Sr isotopic evidence, and implications for Phanerozoic crustal growth. *Chemical Geology* 138, 135–159.
- Han, B.F., He, G.Q., Wang, S.G., Hong, D.W., 1998. Post-collisional mantle-derived magmatism and vertical growth of the continental crust in North Xinjiang. *Geological Review* 44, 396–406 (in Chinese with English abstract).
- Han, B.F., He, G.Q., Wang, S., 1999. Post-collisional magmatism: underplating and property of Junggar basin basement. *Science in China (Series D)* 29, 16–21 (in Chinese with English abstract).
- Han, B.F., Ji, J.Q., Song, B., Chen, L.H., Zhang, L., 2006. Late Paleozoic vertical growth of continental crust around the Junggar Basin, Xinjiang, China (part I): timing of post-collisional plutonism. *Acta Petrologica Sinica* 22, 1077–1086 (in Chinese with English abstract).
- Han, B.F., Guo, Z.J., He, G.Q., 2010. Timing of major suture zones in North Xinjiang, China: constraints from stitching plutons. *Acta Petrologica Sinica* 26, 2233–2246 (in Chinese with English abstract).
- Harris, C., Bell, J.D., Atkins, F.B., 1982. Isotopic composition of lead and strontium in lavas and coarse-grained blocks from Ascension Island, South Atlantic. *Earth and Planetary Science Letters* 60, 79–85.
- Hofmann, A.W., 1988. Chemical differentiation of the Earth: the relationship between mantle, continental crust, and oceanic crust. *Earth and Planetary Science Letters* 90, 297–314.
- Ionov, D.A., Hofmann, A.W., 1995. Nb-Ta-rich mantle amphiboles and micas: implications for subduction-related metasomatic trace element fractionations. *Earth and Planetary Science Letters* 131, 341–356.
- Irvine, T.N., Baragar, W.R.A., 1971. A guide to the chemical classification of the common volcanic rocks. *Canadian Journal of Earth Sciences* 8, 523–548.
- Jung, S., Mezger, K., Hoernes, S., 1998. Petrology and geochemistry of syn- to post-collisional metaluminous A-type granites – a major and trace element and Nd-Sr-Pb-O-isotope study from the Proterozoic Damara Belt, Namibia. *Lithos* 45, 147–175.
- King, P.L., White, A.J.R., Chappell, B.W., Allen, C.M., 1997. Characterization and origin of aluminous A-type granites from the Lachlan Fold Belt, Southeastern Australia. *Journal of Petrology* 38, 371–391.
- Kuibida, M.I., Kruk, N.N., Vladimirov, A.G., Polyanskii, N.V., Nikolaeva, I.V., 2009. U-Pb isotopic age, composition, and sources of the plagiogranites of the Kalba range, Eastern Kazakhstan. *Doklady Earth Sciences* 424, 72–76.
- Li, T., 1976. Chemical element abundances in the earth and its major shells. *Geochimica* 3, 167–174 (in Chinese with English abstract).
- Li, X.H., 1997. Geochemistry of the Longsheng Ophiolite from the southern margin of Yangtze Craton, SE China. *Geochemical Journal* 31, 323–337.
- Li, H.Q., Chen, F.W., Cai, H., 2000. Study on Rb-Sr isotopic ages of gold deposits in West Junggar, Xinjiang. *Acta Geologica Sinica* 74, 181–192 (in Chinese with English abstract).
- Li, X.F., Mao, W., Wang, G., Wang, M., Li, Y.L., Ren, M.C., Xiao, R., Feng, Z.H., Yang, F., 2013. The geology and the ages of Baiyanghe Be-U deposit in Xinjiang province, northwest China. Abstracts Papers to be Presented at the Biennial Meetings of Society for Geology Applied to Mineral Deposits, Uppsala, Sweden, August 12–15, 2013, vol. 4, pp. 1605–1607.
- Litvinovsky, B.A., Jahn, B., Zanvilevich, A.N., Saunders, A., Poulain, S., Kuzmin, D.V., Reichow, M.K., Titov, A.V., 2002. Petrogenesis of syenite–granite suites from the Bryansk Complex (Transbaikalia, Russia): implications for the origin of A-type granitoid magmas. *Chemical Geology* 189, 105–133.
- Loiselle, M.C., Wones, D.S., 1979. Characteristics and origin of anorogenic granites. *Geological Society of America* 11, 468.
- Long, X.P., Sun, M., Yuan, C., Xiao, W.J., Chen, H.L., Zhao, Y.J., Cai, K.D., Li, J.L., 2006. Genesis of Carboniferous volcanic rocks in the eastern Junggar: constraints on the closure of the Junggar Ocean. *Acta Geologica Sinica* 22, 31–40 (in Chinese with English abstract).
- Ma, H.F., Yi, L.S., Xiu, X.Q., 2010. Research on evaluation of uranium and beryllium resource potential in Xiemisitan area, Xinjiang Uyghur Autonomous Region. Internal Report, pp. 1–161 (in Chinese with English abstract).
- Ma, C., Xiao, W., Windley, B.F., Zhao, G., Han, C., Zhang, J.E., Luo, J., Li, C., 2012. Tracing a subducted ridge–transform system in a late Carboniferous accretionary prism of the southern Altaiads: orthogonal sanukitoid dyke swarms in Western Junggar, NW China. *Lithos* 140–141, 152–165.
- Mao, W., Wang, G., Li, X.F., Wang, M., Xiao, R., 2013. A study of fluid inclusions in Baiyanghe U-Be deposit, Xinjiang. *Mineral Deposits* 32, 1026–1034 (in Chinese with English abstract).
- Middlemost, E.A.K., 1994. Naming materials in the magma/igneous rock system. *Earth-Science Reviews* 37, 215–224.
- Mingram, B., Trumbull, R.B., Littman, S., Gerstenberger, H., 2000. A petrogenetic study of anorogenic felsic magmatism in the Cretaceous Paresis ring complex, Namibia: evidence for mixing of crust and mantle-derived components. *Lithos* 54, 1–22.
- Mushkin, A., Navon, O., Halicz, L., Harrmann, G., Stein, M., 2003. The petrology of A-type magmas from the Ammar Massif, Sourthern Israel. *Journal of Petrology* 14, 815–832.
- Pearce, J.A., Harris, N.B.W., Tindle, A.G., 1984. Trace element discrimination diagrams for the tectonic interpretation of granitic rocks. *Journal of Petrology* 25, 956–983.
- Sengör, A.M.C., Natal'in, B.A., Burtman, V.S., 1993. Evolution of the Altaiid tectonic collage and Paleozoic crustal growth in Eurasia. *Nature* 364, 299–307.
- Shen, X.M., Zhang, H.X., Wang, Q., Wyman, D.A., Yang, Y.H., 2011. Late Devonian–Early Permian A-type granites in the southern Altay Range, Northwest China: petrogenesis and implications for tectonic setting of “A2-type” granites. *Journal of Asian Earth Sciences* 42, 986–1007.
- Shen, P., Shen, Y.C., Li, X.H., Pan, H.D., Zhu, H.P., Meng, L., Dai, H.W., 2012. Northwestern Junggar Basin, Xiemisitan Mountains, China: a geochemical and geochronological approach. *Lithos* 140, 103–118.
- Song, B., Li, J.Y., Zhang, J., Zhu, Z.X., Wang, Y., Xu, X., 2011. Zircon SHRIMP U-Pb age of Targen monzogranite in western Junggar, Xinjiang, China: initial time of left-lateral slip of the Tuoli fault. *Geological Bulletin of China* 30, 19–25 (in Chinese with English abstract).
- Su, Y.P., Tang, H.F., 2005. Trace element geochemistry of A-type granites. *Bulletin of Mineralogy, Petrology and Geochemistry* 24, 245–251 (in Chinese with English abstract).
- Su, Y.P., Tang, H.F., Hou, G.S., Liu, C.Q., 2006. Geochemistry of aluminous A-type granites along Darabut tectonic belt in western Junggar, Xinjiang. *Geochimica* 35, 1–5 (in Chinese with English abstract).
- Sun, S.S., McDonough, W.F., 1989. Chemical and isotopic systematics of oceanic basalts: implications for mantle composition and processes. *Geological Society, London, Special Publications* 42, 313–345.
- Tang, G.J., Wang, Q., Zhao, Z.H., Wyman, D.A., Chen, H.H., Jia, X.H., Jiang, Z.Q., 2009. Geochronology and geochemistry of the ore-bearing porphyries in the Baogutu area (Western Junggar): petrogenesis and their implications for tectonics and Cu-Au mineralization. *Earth Science* 34, 56–74 (in Chinese with English abstract).
- Tang, G.J., Wang, Q., Wyman, D.A., Li, Z.X., Zhao, Z.H., Jia, X.H., Jiang, Z.Q., 2010a. Ridge subduction and crustal growth in the Central Asian Orogenic Belt: evidence from Late

- Carboniferous adakites and high-Mg diorites in the western Junggar region, northern Xinjiang (west China). *Chemical Geology* 277, 281–300.
- Tang, G.J., Wang, Q., Wyman, D.A., Sun, M., Li, Z.X., Zhao, Z.H., Sun, W.D., Jia, X.H., Jiang, Z.Q., 2010b. Geochronology and geochemistry of Late Paleozoic magmatic rocks in the Lamasu-Dabate area, northwestern Tianshan (west China): evidence for a tectonic transition from arc to post-collisional setting. *Lithos* 119, 393–411.
- Tang, G.J., Wyman, D.A., Wang, Q., Li, J., Li, Z.X., Zhao, Z.H., Sun, W.D., 2012. Asthenosphere–lithosphere interaction triggered by a slab window during ridge subduction: trace element and Sr–Nd–Hf–Os isotopic evidence from Late Carboniferous tholeiites in the western Junggar area (NW China). *Earth and Planetary Science Letters* 329, 84–96.
- Tiepolo, M., Bottazzi, P., Foley, S.F., Oberti, R., Vannucci, R., Zanetti, A., 2001. Fractionation of Nb and Ta from Zr and Hf at mantle depths: the role of titanian pargasite and kaersutite. *Journal of Petrology* 42, 221–232.
- Tiepolo, M., Oberti, R., Zanetti, A., Vannucci, R., Foley, S.F., 2007. Trace-element partitioning between amphibole and silicate melt. *Reviews in Mineralogy and Geochemistry* 67, 417–452.
- Turner, S.P., Foden, J.D., Morrison, R.S., 1992. Derivation of some A-type magmas by fractionation of basaltic magma—an example from the Padthaway Ridge, South Australia. *Lithos* 28, 151–179.
- Vladimirov, A.G., Krug, N.N., Khromykh, S.V., Polyansky, O.P., Chervov, V.V., Vladimirov, V.G., Travin, A.V., Babin, G.A., Kuibida, M.L., Vladimirov, V.D., 2008. Permian magmatism and lithospheric deformation in the Altai caused by crustal and mantle thermal processes. *Russian Geology and Geophysics* 49, 468–479.
- Volkert, R.A., Feigenson, M.D., Patino, L.C., Delaney, J.S., Drake, A.A., 2000. Sr and Nd isotopic compositions, age and petrogenesis of A-type granitoids of the Vernon Supersuite, New Jersey Highlands, USA. *Lithos* 50, 325–347.
- Wang, F.T., 2006. The Paleogeographic and Geo-ecological Atlas of Xinjiang Uygur Autonomous Region. SinoMaps Press, Beijing p. 226 (in Chinese with English abstract).
- Wang, B., Chen, Y., Zhan, S., Shu, L., Faure, M., Cluzel, D., Charvet, J., Laurent-Charvet, S., 2007a. Primary Carboniferous and Permian paleomagnetic results from the Yili Block (NW China) and their implications on the geodynamic evolution of Chinese Tianshan Belt. *Earth and Planetary Science Letters* 263, 288–308.
- Wang, Q., Wyman, D., Zhao, Z., Xu, J., Bai, Z., Xiong, X., Dai, T., Li, C., Chu, Z., 2007b. Petrogenesis of Carboniferous adakites and Nb-enriched arc basalts in the Alataw area, northern Tianshan Range (western China): implications for Phanerozoic crustal growth in the Central Asia orogenic belt. *Chemical Geology* 236, 42–64.
- Wang, M., Li, X.F., Wang, G., Li, Y.L., Shi, Z.L., Lu, K.G., 2012. Geological characteristics of Baiyanghe Beryllium–Uranium deposits in Xuemisitan volcanic belt, Xinjiang. *Mineral Exploration* 3, 34–40 (in Chinese with English abstract).
- Whalen, J.B., 2005. A-type granites: N25 years later. *Geochimica et Cosmochimica Acta* 69, A84.
- Whalen, J.B., Currie, K.L., Chappell, B.W., 1987. A-type granites: geochemical characteristics, discrimination and petrogenesis. *Contributions to Mineralogy and Petrology* 95, 407–419.
- Wickham, S.M., Alberts, A.D., Zanvilevich, A.N., Litvinovsky, B.A., Bindeman, I.N., Schauble, E.A., 1996. A stable isotope study of anorogenic magmatism in East Central Asia. *Journal of Petrology* 37, 1063–1095.
- Xu, Z., Han, B.F., Ren, R., Zhou, Y.Z., Zhang, L., Chen, J.F., Su, L., Li, X.H., Liu, D.Y., 2012. Ultramafic–mafic mélange, island arc and post-collisional intrusions in the Mayile Mountain, West Junggar, China: Implications for Paleozoic intra-oceanic subduction–accretion process. *Lithos* 132–133, 141–161.
- Yang, J.H., Wu, F.Y., Chung, S.L., Wilde, S.A., Chu, M.F., 2006. A hybrid origin for the Qianshan A-type granite, northeast China: geochemical and Sr–Nd–Hf isotopic evidence. *Lithos* 89, 89–106.
- Yang, G.X., Li, Y.J., Gu, P.Y., Yang, B.K., Tong, L.L., Zhang, H.W., 2012. Geochronological and geochemical study of the Darbut Ophiolitic Complex in the West Junggar (NW China): implications for petrogenesis and tectonic evolution. *Gondwana Research* 21, 1037–1049.
- Yin, J.Y., Yuan, C., Sun, M., Long, X.P., Zhao, G.C., Wong, K.P., Geng, H., Cai, K., 2010. Late Carboniferous high-Mg dioritic dikes in Western Junggar, NW China: geochemical features, petrogenesis and tectonic implications. *Gondwana Research* 17, 145–152.
- Yin, J.Y., Yuan, C., Wang, Y.J., Long, X.P., Guan, Y.L., 2011. Magmatic records on the Late Paleozoic tectonic evolution of Western Junggar, Xinjiang. *Geotectonica et Metallogenesis* 35, 278–291 (in Chinese with English abstract).
- Zhang, X., Zhang, H., 2014. Geochronological, geochemical, and Sr–Nd–Hf isotopic studies of the Baiyanghe A-type granite porphyry in the Western Junggar: Implications for its petrogenesis and tectonic setting. *Gondwana Research* 25, 1554–1569.
- Zhang, L.G., Wang, K.F., Chen, Z.S., Liu, J.X., Li, Z.T., 1993. Pb isotope composition and partition of Pb isotope province of East China Mesozoic granites. *Chinese Science Bulletin* 38, 254–257 (in Chinese with English abstract).
- Zhang, J.E., Xiao, W.J., Han, C.M., Guo, Q.Q., Mao, Q.G., Ao, S.J., 2010. Magmatism of mid-oceanic ridge subduction during Carboniferous in Western Junggar: evidence from Maliya ophiolite. *Acta Petrologica Sinica* 26, 3272–3282 (in Chinese with English abstract).
- Zhang, J.E., Xiao, W.J., Han, C.M., Ao, S.J., Yuan, C., Sun, M., Geng, H.Y., Zhao, G.C., Guo, Q.Q., Ma, C., 2011a. Kinematics and age constraints of deformation in a Late Carboniferous accretionary complex in Western Junggar, NW China. *Gondwana Research* 19, 958–974.
- Zhang, J.E., Xiao, W.J., Han, C.M., Mao, Q.G., Ao, S.J., Guo, Q.Q., Ma, C., 2011b. A Devonian to Carboniferous intra-oceanic subduction system in Western Junggar, NW China. *Lithos* 125, 592–606.
- Zhao, L., He, G., 2013. Tectonic entities connection between West Junggar (NW China) and East Kazakhstan. *Journal of Asian Earth Sciences* 72, 25–32.